Critical Strains in Poly(ϵ-caprolactone) and Blends with Poly(vinyl methyl ether) and Poly(styrene-*co*-acrylonitrile)

Y. Men*,† and G. Strobl

Physikalisches Institut, Albert-Ludwigs-Universität, 79104 Freiburg, Germany

Received December 12, 2002; Revised Manuscript Received January 28, 2003

ABSTRACT: The deformation properties under a tensile load of poly(ϵ-caprolactone) (PCL) were compared to those of PCL/PVME and PCL/SAN mixtures. The critical strains at the end of the Hooke range (point A) and at the yield point (point B) remain unchanged. The critical strain marking the beginning of a disintegration of the blocklike crystallites and a fibril formation (point C) is generally affected for the PCL/PVME mixture only slightly but for the PCL/SAN mixtures quite strongly. As it appears, the swelling of the amorphous regions by PVME does not much change the entanglement density, whereas an inclusion of SAN does this and thus reduces the shear modulus. For a smaller modulus the strain required to produce the stress leading to a disintegration of the blocks becomes larger. Prior to the mechanical tests, a structural characterization of the different blends was carried out by SAXS and DSC. As was found, the presence of a second noncrystallizable compound does not change the crystal thickness and results only in an expansion of the amorphous intercrystalline regions.

1. Introduction

Poly(ϵ-caprolactone) (PCL) is a crystallizable polymer which forms in the melt homogeneous mixtures with a variety of other polymers, with poly(vinyl methyl ether) (PVME),[1−3] poly(styrene-*co*-acrylonitrile) (SAN),[4,5] poly(vinyl chloride),[6,7] or methacrylate polymers,[8,9] to select only the best known examples. PCL is therefore a natural candidate to investigate how mixing affects the crystallization and the mechanical properties of a polymer system. Several groups used it to study the changes in the spherulitic morphology and in the crystallization rates or effects on the nanoscopic structure (compare, for example, refs 1, 10, and 11 and references therein). This paper addresses mechanical properties, more specifically, the yielding behavior under a tensile load. Employing a video-controlled tensile testing machine, we recently measured for various semicrystalline polymers, polyethylenes,[12,13] polypropylenes,[14] and poly(1-butene),[15] true stress−strain curves for constant strain rates. As it turned out, these curves demonstrate the existence of a common scenario: For each polymer three critical strains are found where the deformation mechanism changes, and interestingly, these strains are invariant against variations in the temperature, the degree of crystallinity, or the strain rate. On the basis of numerous observations, we associate the three critical points with (1) the onset of local flow processes at the end of the Hooke range with ideal elasticity ("point A"), (2) a collective onset of slip processes of the crystal blocks composing the crystal lamellae, which determines the yield point ("point B"), and (3) the beginning of a disintegration of the crystal blocks which is followed by a fibril formation ("point C").

While the yield point B is a property of the skeleton of the crystal blocks only, point C depends on properties both of the crystals—their binding energy—and of the entangled network which produces the force resulting in the block disintegration.[16,17] We therefore expect that a change in the network properties leads to a change in the location of point C. An obvious way to modify the network properties, i.e., the entanglement density, is blending, and the mixtures which can be prepared for PCL offer this possibility.

We chose blends with PVME and SAN and investigated their deformation properties in tensile tests. The results are given in the following. Before starting with the mechanical experiments, the samples were structurally characterized by small-angle X-ray scattering (SAXS) experiments and DSC runs. The subsequent yielding tests began with pure PCL and were then extended to various mixtures with PVME and SAN.

2. Experimental Section

2.1. Samples. The PCL under study was supplied by Aldrich Chemical Co. and had molar masses $M_n = 42\,000$ and $M_w = 65\,000$. PVME was obtained from Polyscience Inc. and SAN (25% AN) from the BASF AG ($M_n = 100\,000$ and $M_w = 193\,000$). PCL/SAN blends were prepared by mixing the two components at 160 °C for about 10 min in a mini-extruder. In the case of the PCL/PVME blends mixing was achieved in a THF solution. The THF was evaporated at room temperature by first keeping samples for 12 h in air and then putting the blend for 72 h in a vacuum oven. Samples for the measurements were obtained by pressing the melt between two glass plates. Crystallization occurred in uncontrolled manner during a slow cooling to room temperature. The dog-bone samples used in the mechanical tests were cut out of sheets with a thickness of 0.3−0.5 mm.

2.2. Techniques. 2.2.1. Small-Angle X-ray Scattering. The crystallinities, crystal thicknesses, and long spacings in mixtures of PCL with a noncrystallizable second polymer differ usually from those found in pure PCL. Before carrying out comparative mechanical tests, it is therefore necessary to determine the structure parameters of the mixtures. This can be accomplished by small-angle X-ray scattering experiments employing standard procedures. We carried out SAXS experiments with the aid of a Cu Kα X-ray tube employing a Kratky compact camera. By applying a desmearing procedure and measuring the primary beam intensity with a moving slit system, we obtained pinhole scattering curves $I(s)$ in absolute

† New address: BASF Aktiengesellschaft, Polymer Physics, 67056 Ludwigshafen, Germany.

* Corresponding author.

10.1021/ma025955b CCC: $25.00
Published on Web 02/28/2003

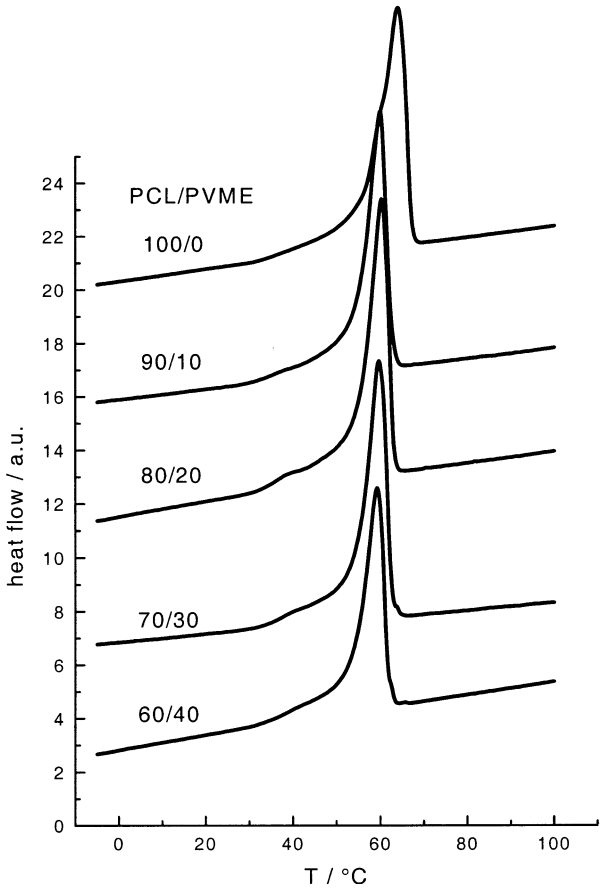

Figure 1. Series of PCL/PVME blends: DSC melting curves of the investigated samples (heating rate: 10 K min^{-1}).

values. From the position of the maximum in the Lorentz-corrected curve $I(s)s^2$, we derived the long spacing d_{ac}. Crystal thicknesses d_c generally show up as peaks in the interface distance distribution function which is identical with the second derivative of the one-dimensional electron density correlation function, $K''(z)$. $K(z)$ and $K''(z)$ can be calculated in a straightforward manner by Fourier transformations of the scattering curve (the details were repeatedly described, e.g., in refs 18 and 19).

The ratio of the crystal thickness and the long-spacing yields the linear crystallinity

$$\phi_l = \frac{d_c}{d_{ac}}$$

Basically ϕ_l represents a volume fraction crystallinity. If the sample is not completely filled with stacks of lamellae, ϕ_l is larger than the bulk crystallinity. A comparison of the DSC crystallinity with ϕ_l can therefore be used to judge whether one deals with a homogeneous or a macroscopically phase-separated sample.

2.2.2. Differential Scanning Calorimetry. DSC experiments were performed in a Perkin-Elmer DSC-4 at a heating rate of 10 K/min. Weight fraction crystallinities ϕ_w were derived from the heat of fusion ΔH by calculating the ratio $\Delta H/\Delta H_{id}$ to the ideal value $\Delta H_{id} = 157$ J g^{-1}.

2.2.3. Mechanical Stretching and Recovery Tests. We used in our experiments the Hencky measure of strain

$$\epsilon_H = \ln \lambda$$

where λ denotes the extension ratio. Following the procedure developed by G'Sell,[20] true stress−strain curves were measured using an INSTRON 4301 machine equipped with a video control which maintains a constant local strain rate in the neck center. This can be accomplished by an imaging of the neck profile with the aid of a CCD camera. Assuming a constant sample volume during the deformation, the local strain in the center of the neck can be derived from the minimum diameter and the stretching rate readjusted so that the strain rate $\dot{\epsilon}_H$ is kept constant. The related local stress can be simultaneously determined. The temperature was controlled using an INSTRON 3111 heating chamber with a range from room temperature up to 200 °C.

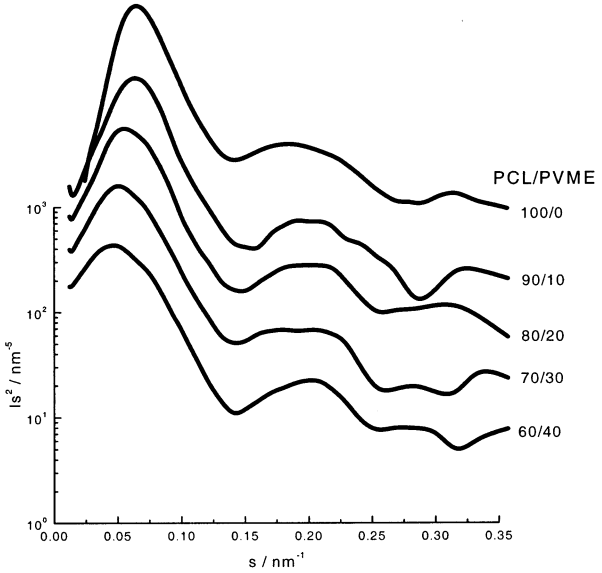

Figure 2. Series of PCL/PVME blends: SAXS curves Is^2 vs s. The curve for the 60/40 blend is in the correct position; the other curves are vertically shifted by constant factors.

Elastic properties in the deformed state were derived from the following:

(i) Step-cycle tests, which combine a stepwise stretching of the samples with unloading−reloading cycles. The sample is extended step-by-step with a constant Hencky strain rate. After each step, the sample's speed of extension is inverted and used to contract the sample until a stress of zero is achieved. Thereupon, the sample is extended again, at this given speed, until it rereaches the point at which it left the regulated curve.

(ii) Determinations of the free shrinkage after unloading. After stretching with a constant strain rate to a predetermined end strain, the lower clamp is released, and the change in the sample width is monitored. Both methods lead to a partitioning of the total strain into a reversible and an irreversible part.

3. Results

3.1. Structure Characterization. 3.1.1. PCL/PVME Mixtures. Figure 1 displays DSC thermograms obtained during a heating for all the mixtures under study. Above 65 °C melting is completed for all mixtures. We find also a constant melting point; only for the pure PCL is it 4 deg higher, probably due to a one-time melting−recrystallization process.

Figure 2 presents the Lorentz-corrected SAXS curves obtained for the various mixtures. Applying Bragg's law on the location of the first peak, the long spacing d_{ac} is obtained. d_{ac} obviously increases with increasing PVME content. Figure 3 displays the interface distance distribution functions derived from the scattering curves. The first peaks relate to the crystallites; the location of the maximum yields the crystal thickness d_c. As to be noted, d_c does not change and is constantly at 7 nm for PCL and all mixtures with PVME. Figure 4 collects these values together with the long spacings from Figure 2,

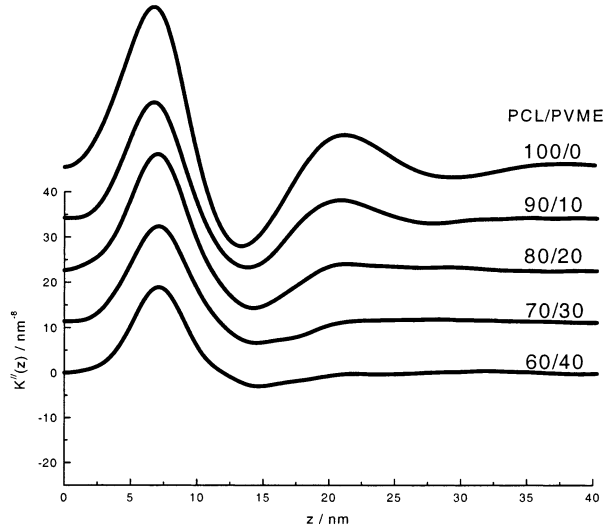

Figure 3. Interface distance distribution functions derived from the SAXS curves in Figure 2. The curve for the 60/40 blend is in the correct position; the other curves are vertically shifted by constant increments.

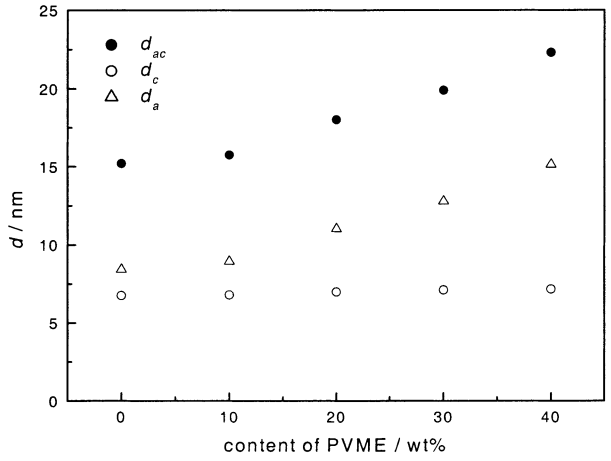

Figure 4. Series of PCL/PVME blends: crystal thicknesses d_c, long spacings d_{ac}, and thicknesses of the amorphous layers d_a derived from the SAXS data.

and the derived thicknesses of the intercrystalline amorphous layers d_a are given by

$$d_a = d_{ac} - d_c$$

The crystallinities ϕ_c derived from the heats of fusion are given in Figure 5. The sample crystallinity decreases when the fraction of PVME, x_{PVME}, gets larger. Note that the fraction of crystallized PCL, given by ϕ_c/x_{PCL} and also included in the figure, increases. This confirms a similar observation by Oudhuis et al.[1] Figure 5 shows three crystallinity values: (i) the sample crystallinity as determined by SAXS, (ii) the sample crystallinity as determined by DSC, and (iii) the fraction of crystallized PCL. The sample crystallinities determined by SAXS and DSC agree within the error limits of the measurement.

3.1.2. PCL/SAN Mixtures. Figures 6−10 display the results of analogous measurements carried out for the PCL/SAN mixtures. One again observes an increase of d_{ac} with the volume content of the noncrystallizable component x_{SAN} (compare Figure 7) and an invariance of the crystal thickness d_c (Figure 8). The fraction of crystallized PCL, ϕ_c/x_{PCL}, is now constantly 0.5. One

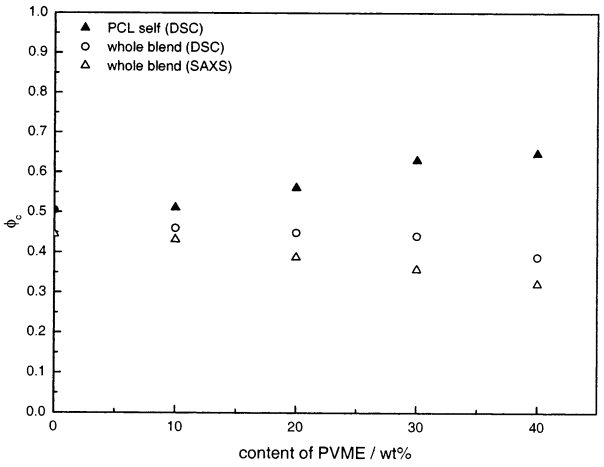

Figure 5. Series of PCL/PVME blends: mass fraction of crystallites in the sample (○) and fraction of crystallized PCL (▲), derived from the heat of fusion; volume fraction of crystallites within the stacks (△) obtained by SAXS.

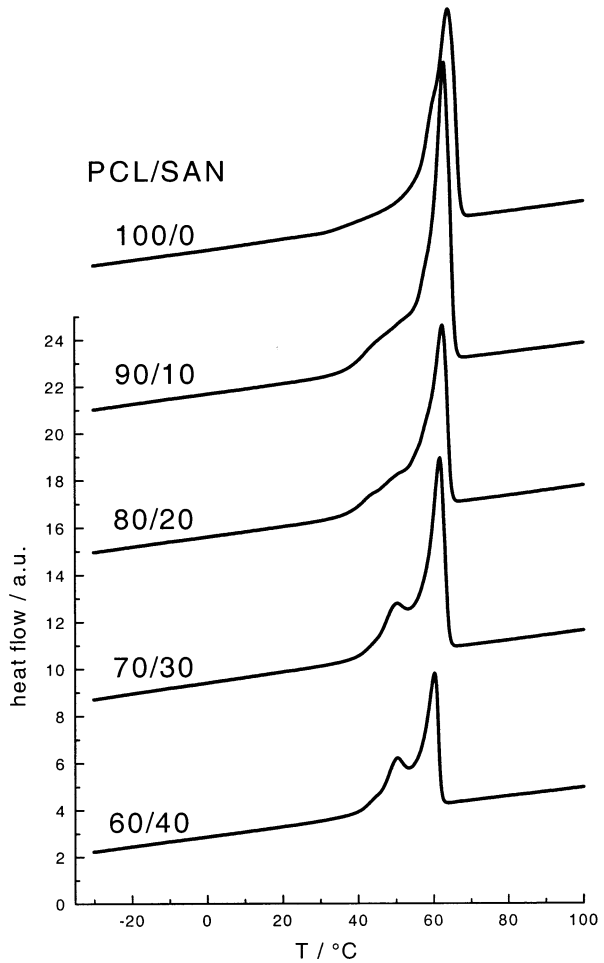

Figure 6. Series of PCL/SAN blends: DSC melting curves obtained with a heating rate of 10 K min^{-1}.

again finds an agreement between the crystallinities deduced from DSC and SAXS. Notably, one finds a second low-temperature melting peak in DSC runs for blends with high SAN content (Figure 6). The meaning of this second peak is obvious. It represents the melting of a group of crystallites with less stability than that of lamellae.[21] It locates always just a couple degrees above the crystallization temperature. A closer look at Figures 1 and 6 reveals that melting always sets in earlier than the main melting peak. Beside the obvious peak in

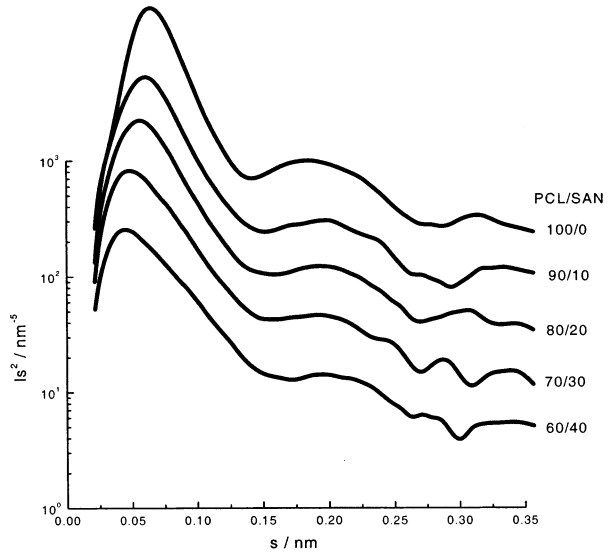

Figure 7. Series of PCL/SAN blends: SAXS curves Is^2 vs s.

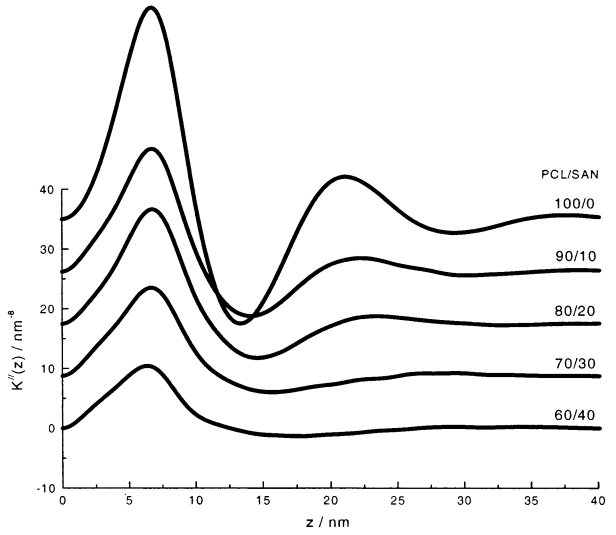

Figure 8. Interface distance distribution functions derived from the SAXS curves in Figure 7.

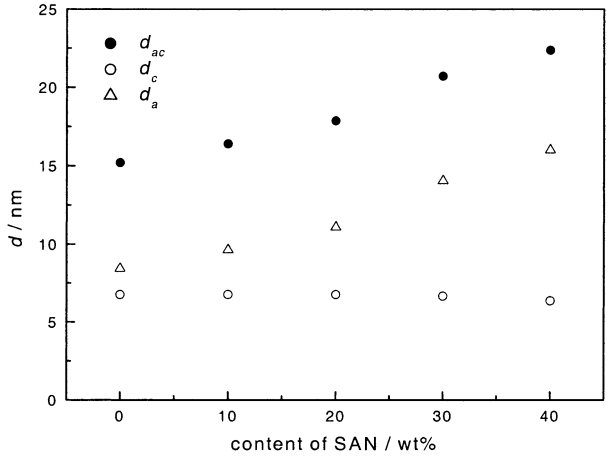

Figure 9. Series of PCL/SAN blends: crystal thicknesses d_c, long spacings d_{ac}, and thicknesses of the amorphous layers d_a derived from the SAXS data.

blends with high SAN content, it appears as a shoulder at the low-temperature side of the main melting peak for all blends of PCL/PVME and for PCL/SAN blends with 10 and 20 wt % SAN or a continuous increase in heat flow for pure PCL sample. Blending with a second amorphous component hinders the formation of perfect lemallae and thus increases the amount of the less stable crystallites. This becomes more pronounced in PCL/SAN blends because of a higher viscosity in their amorphous phase which makes the perfection of the crystalline lamellae more difficult.

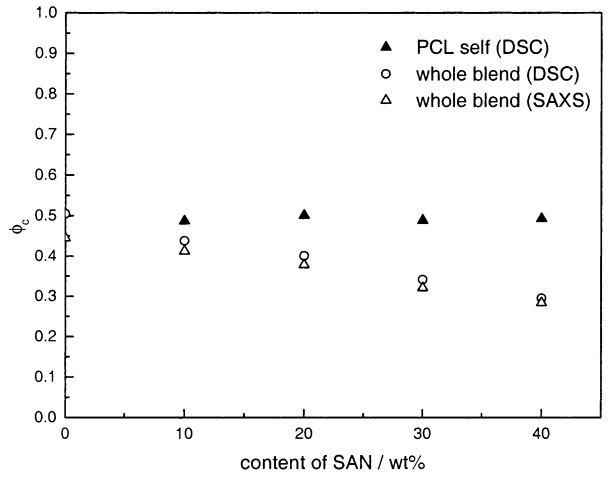

Figure 10. Series of PCL/SAN blends: mass fraction of crystallites in the sample (○) and mass fraction of crystallized PCL (▲), derived from the heat of fusion; volume fraction of crystallites within the stacks (△) obtained by SAXS.

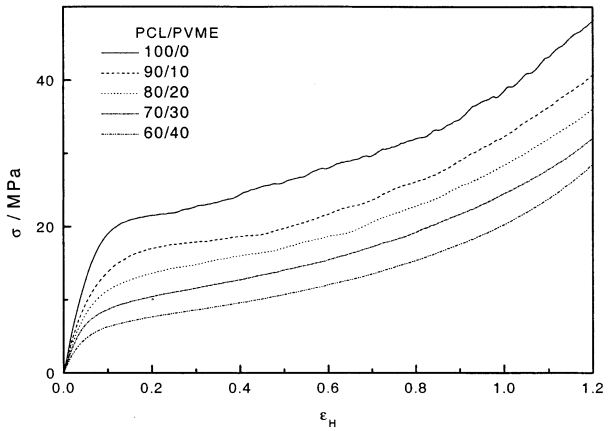

Figure 11. Series of PCL/PVME blends: true stress−true strain relationships measured under video control during tensile deformations with a strain rate $\dot{\epsilon}_H = 5 \times 10^{-3}$ s^{-1}.

3.2. Tensile Deformation Behavior. The deformation and yielding properties during a drawing were studied for all samples by (i) a measurement of the true stress−strain curve carried out—as all samples showed necking—by employing the video control and thereby fixing the strain rate in the center of the neck to $\dot{\epsilon}_H = 5 \times 10^{-3}$ s^{-1} and (ii) a registration of the strain recovery, performing step-cycle and free shrinkage tests.

3.2.1. Stress−Strain Curves. Figure 11 presents for all PCL/PVME mixtures the relationship between the true stress and the (Hencky) strain, $\sigma(\epsilon_H)$. One observes a systematic variation between the different samples. Above the respective yield points one finds an essentially invariant curve shape; curves are just shifted parallel to each other. As expected, stresses decrease with increasing x_{PVME}. The shape invariance already indicates that the critical strain at the yield point, ϵ_H(B), and at the onset of fibrillation, ϵ_H(C), are essentially constant throughout the series, i.e., not much affected by the mixing.

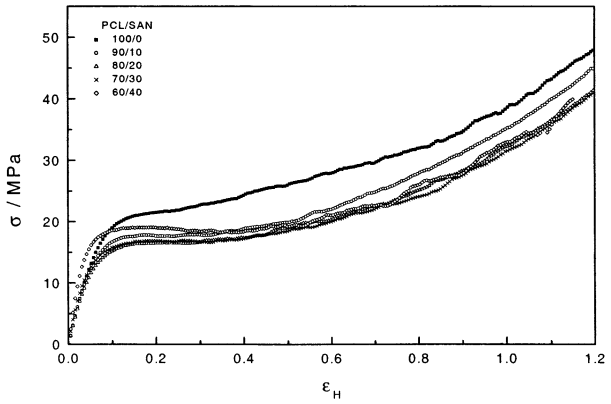

Figure 12. Series of PCL/SAN blends at 30 °C: true stress−true strain relationships measured under video control during tensile deformations with a strain rate $\dot{\epsilon}_H = 5 \times 10^{-3}$ s^{-1}.

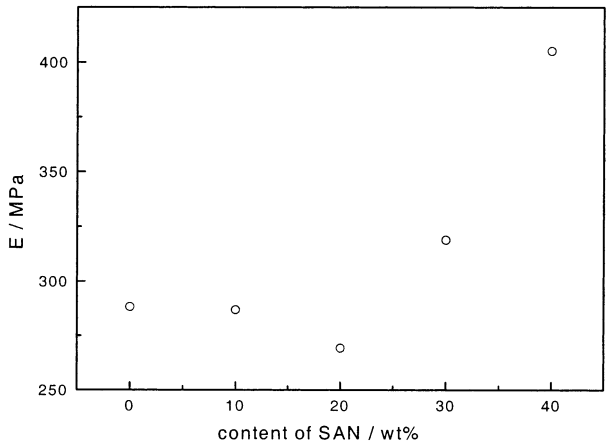

Figure 13. Series of PCL/SAN blends at 30 °C: Young's moduli as given by the slopes at the origin of the stress−strain curves in Figure 12.

Figure 12 shows the same experiment carried out for the PCL/SAN mixtures. The results look different as one cannot see, at first glance, any systematic variation. The reason for that is easily seen: The difference in behavior is caused by the different glass transition temperatures of PVME and SAN, $T_g = -34$ °C for PVME and $T_g = 104$ °C for SAN. In the PCL/PVME mixtures the amorphous regions are always liquid, while, depending on their composition, the PCL/SAN mixture can be highly viscous. Even if the homogeneous melt is fluid, the conditions may change during the crystallization which leads to a reduction of the PCL fraction in the fluid phase and, additionally, during the cooling to room temperature. Measurements of Young's modulus E demonstrate that at higher volume fractions of SAN indeed a freezing occurs. Figure 13 shows the measured values E, with a sharp increase for SAN concentrations above 30%.

The interference of freezing can be avoided by conducting the measurements at an enhanced temperature, e.g., 50 °C. Figure 14 presents the true stress−strain curves then obtained. Now one finds systematic variations with the blend composition. The variations, however, differ from those in the PCL/PVME blends: The shape of the curves above the respective yield points is no longer constant. The strain hardening at higher strains becomes less pronounced if the volume fraction x_{SAN} increases. This change in the curve shapes now speaks against an invariance of ϵ_H(C), and indeed, the strain recovery tests prove that.

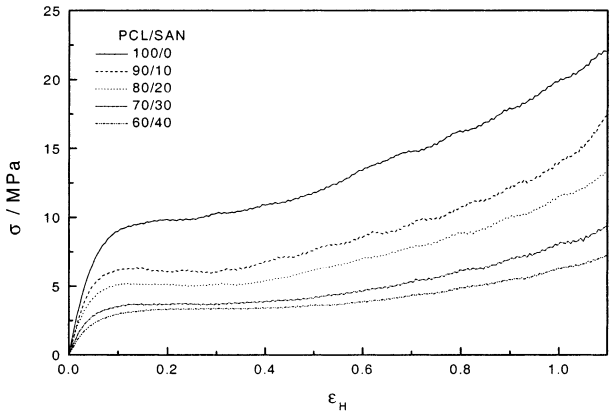

Figure 14. Series of PCL/SAN blends at 50 °C: true stress−true strain relationships measured under video control during tensile deformations with a strain rate $\dot{\epsilon}_H = 5 \times 10^{-3}$ s^{-1}.

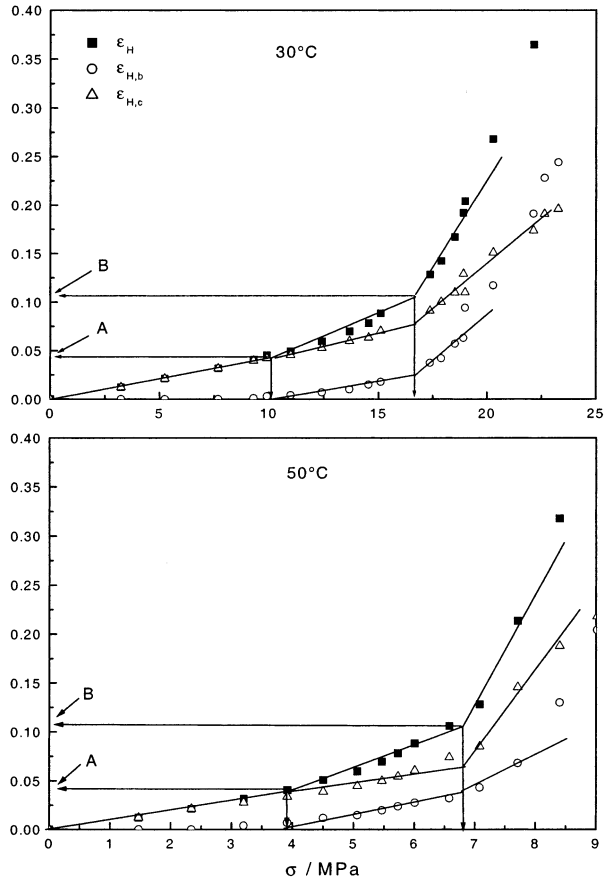

Figure 15. PCL: results of step-cycle tests carried out at 30 and 50 °C: reversible part $\epsilon_{H,c}$ and irreversible part $\epsilon_{H,b}$ of the total strain ϵ_H as a function of the stress. The locations of the critical points A and B are indicated.

3.2.2. Strain Recovery. A partitioning of the strain in a recoverable ("cyclic") and an irreversible ("base") part achieved by step-cycle runs and free shrinkage tests is the best way for the determination of the critical points A (end of Hooke range), B (yield point, onset of collective block slips), and C (block disintegration, caused by the network forces, followed by fibril formation). At first, these experiments were carried out for pure PCL. Figures 15 and 16 display the results of step-cycle runs. The figures give the total strain, the recoverable, and (quasi-)permanent part ϵ_H, $\epsilon_{H,c}$, and $\epsilon_{H,b}$ as a function of the true stress. The critical points A and B are clearly indicated by a break in all three curves. It

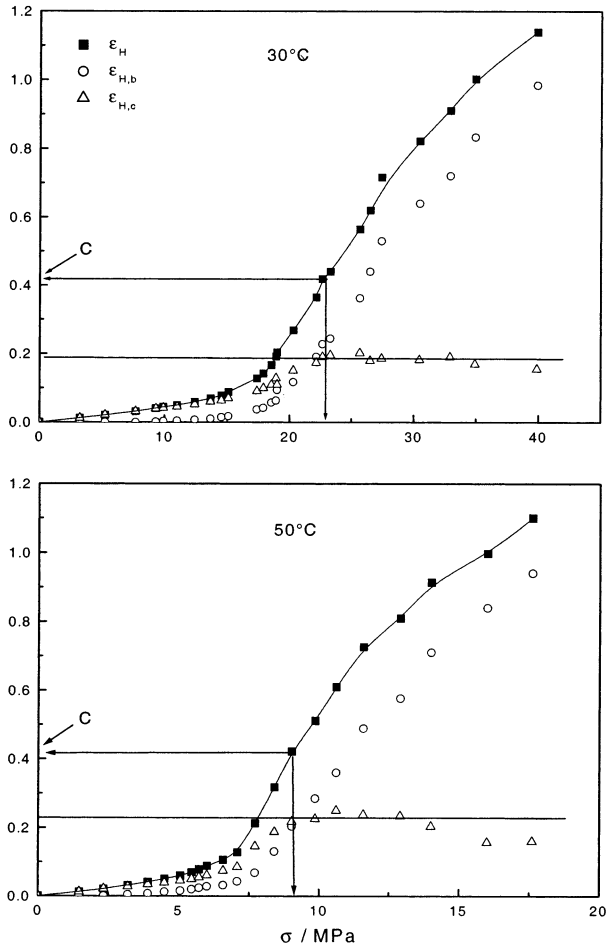

Figure 16. PCL: results of step-cycle tests carried out at 30 and 50 °C. The locations of the critical point C are indicated.

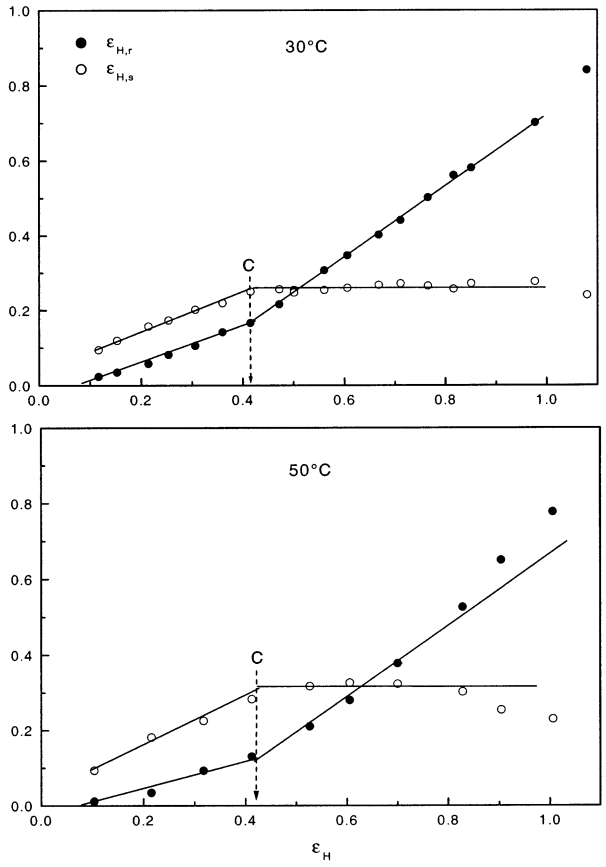

Figure 17. PCL: results of free shrinkage tests carried out at 30 and 50 °C. The locations of the critical point C are indicated.

is a characteristic property of the critical point C that here the recoverable part reaches its maximum value. From thereon $\epsilon_{H,c}$, which describes the sample elasticity, remains at a constant plateau value. This behavior was observed for all systems investigated so far and therefore represents an essential feature of the deformability of partially crystalline polymers. Figure 16 demonstrates that such a point exists again for PCL.

For PE, sPP, and P1B the critical strains turned out as invariant; they did not change neither with temperature nor with the sample crystallinity. For PCL we have a similar observation. Measurements carried out at 50 °C, which are also included in Figures 15 and 16, show unchanged locations of the critical strains at A, B, and C. Note that, on the other hand, stresses change quite remarkably, in the case of point B from 17 to 7 MPa and in the case of point C from 23 to 9 MPa.

Even clearer than in the step-cycle tests the location of point C shows up in free shrinkage measurements with which the total strain, ϵ_H, can be partitioned into the recoverable shrinkaged part, $\epsilon_{H,s}$, and (quasi-)-permanent rest part, $\epsilon_{H,r}$. These are given in Figure 17 and determine the critical strain at C as

$$\epsilon_H(C) = 0.42$$

Do the critical strains change when we mix PCL with PVME or SAN? The first, quite clear result concerns the PCL/PVME blend. As could be already anticipated from Figure 11 with the unchanged curve shapes above the yield point, for these mixtures no essential changes occur. Figures 18−20 present the results of step-cycle and free shrinkage tests for all mixtures. We constantly find

$$\epsilon_H(A) = 0.03-0.04, \quad \epsilon_H(B) = 0.11$$

and for $\epsilon_H(C)$ a minor shift which looks systematic, but still keeps the values in the comparatively small range

$$\epsilon_H(C) = 0.43-0.49$$

Note that at the same time the stresses decrease quite remarkably, $\sigma(A)$ from 9 to 3 MPa, $\sigma(B)$ from 16 to 7 MPa, and $\sigma(C)$ from 19 to 11 MPa between PCL and the PCL/PVME (60/40) mixture.

For the PCL/SAN blends we have different results, not unexpected in view of Figure 14. The recovery tests, now also carried out at 50 °C to avoid effects of a freezing of the amorphous phase, are given in Figures 21 and 22 for two of the mixtures. The critical strains $\epsilon_H(A)$ and $\epsilon_H(B)$ still do not change by the mixing, but the location of point C, $\epsilon_H(C)$, is now clearly affected. One observes a shift from 0.6 to 0.9. Figure 23 displays the dependence of $\epsilon_H(C)$ on the volume content x_{SAN} of the noncrystallizable component. The figure includes also results of measurements carried out at room temperature, where freezing effects in the SAN-rich amorphous phase interfere. In the free shrinkage tests which can use an arbitrarily long time for the strain recovery there is no difference to the results obtained at 50 °C, while a difference arises in the step-cycle runs as these give relaxation processes only a limited time.

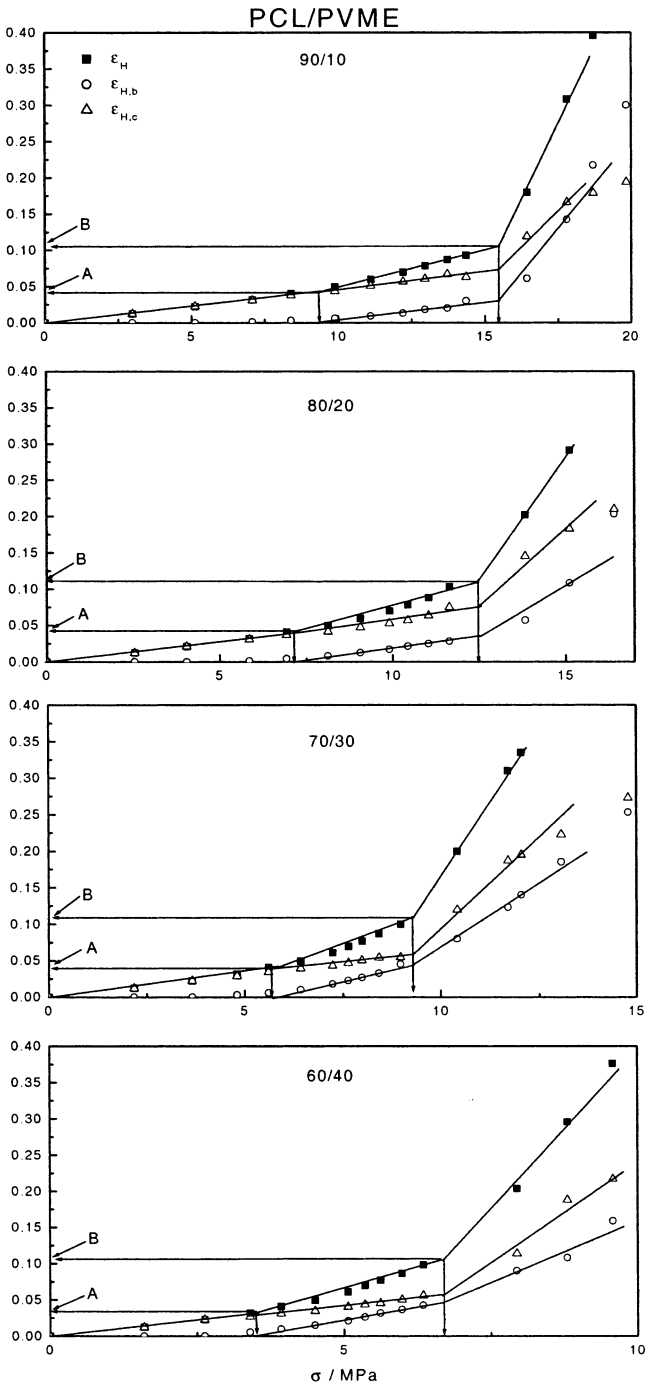

Figure 18. Series of PCL/PVME blends: results of step-cycle tests carried out at 30 °C. The locations of the critical points A and B are indicated.

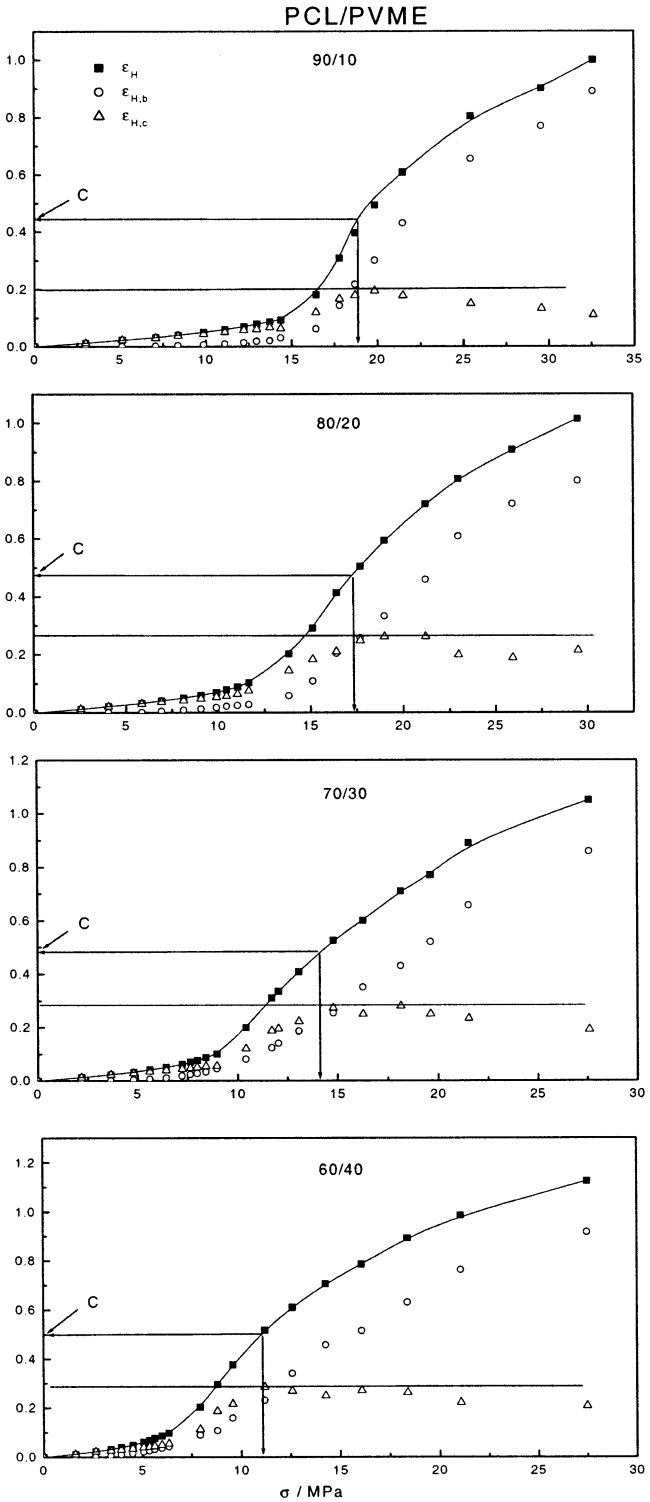

Figure 19. Series of PCL/PVME blends: results of step-cycle tests carried out at 30 °C. The locations of the critical point C are indicated.

4. Discussion

The structural characterization experiments carried out to evaluate the effects of the mixing processes on the crystalline−amorphous structure yielded a simple result: (i) The presence of a noncrystallizable component in the homogeneous melt does not change the thickness of the crystals formed after a cooling; it only leads to an increase in the long spacing. (ii) As we find an agreement between the linear crystallinity ϕ_l from SAXS and the bulk crystallinity ϕ from DSC, we can be sure that crystallization does not induce unmixing processes. The PVME and SAN chains are just incorporated in the amorphous intercrystalline layers and correspondingly thicken them. In the PCL/PVME mixtures, the presence of PVME promotes the crystallization of PCL in the sense that here, compared to the homogeneous PCL, a larger part of PCL crystallizes. No such effect is found for the PCL/SAN mixtures. Here the fraction of crystallized PCL remains constant.

A simple result was also found for the yield point when we compare PCL with the two mixed systems. The critical strain at the yield point, ϵ_H(B), is constantly at 0.11, i.e., is not affected by the blending. The same is found for the critical strain which marks the end of the

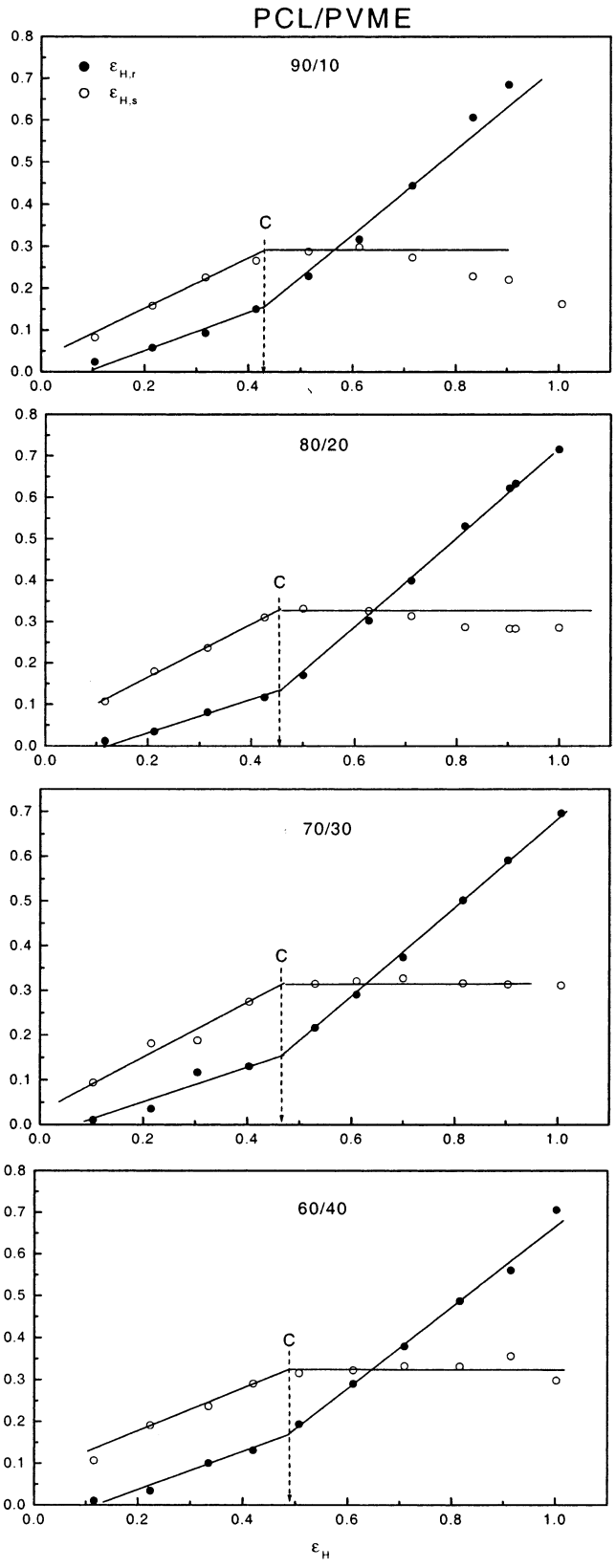

Figure 20. Series of PCL/PVME blends: results of free shrinkage tests carried out at 30 °C. The locations of the critical point C are indicated.

Hooke range, ϵ_H(A), which remains fixed at around 0.04. Different from the strain, the critical stresses σ(B) and σ(A) and consequently also the Young's moduli E are affected by the mixing process. In both blends they decrease with increasing volume fraction of the non-crystallizable component.

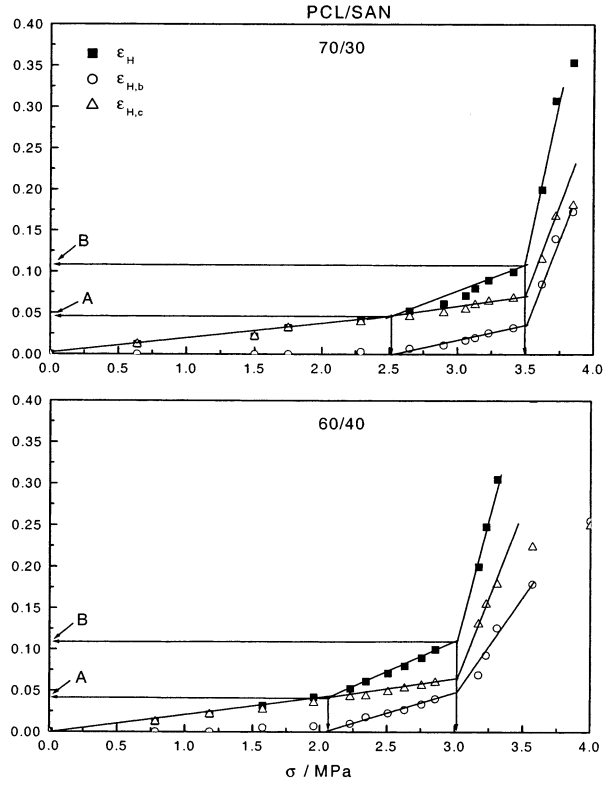

Figure 21. Two PCL/SAN blends: results of step-cycle tests carried out at 50 °C. The locations of the critical points A and B are indicated.

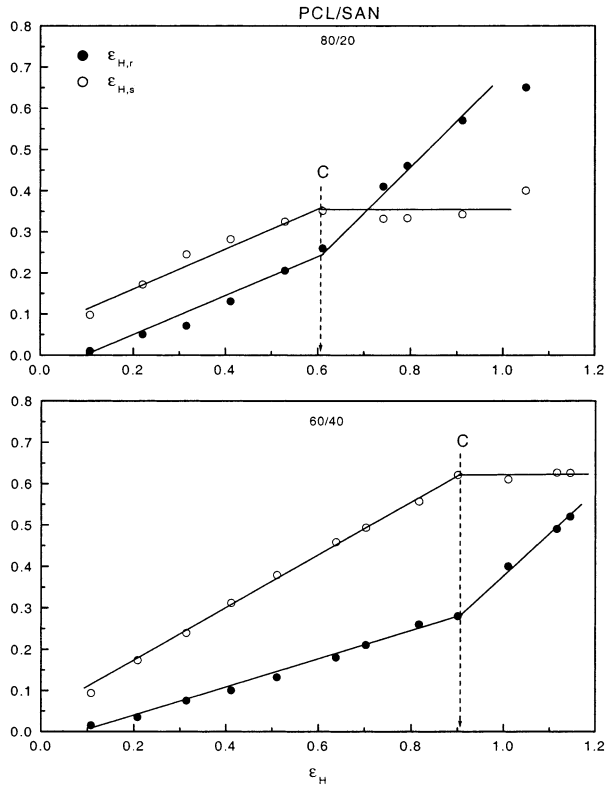

Figure 22. Series of PCL/SAN blends: results of free shrinkage tests carried out at 50 °C. The locations of the critical point C are indicated.

The yield point and the Young's modulus are mainly properties of the stiff skeleton built up by the crystal blocks in the fluid entangled matrix. It was generally found, for all homopolymers investigated so far, that a

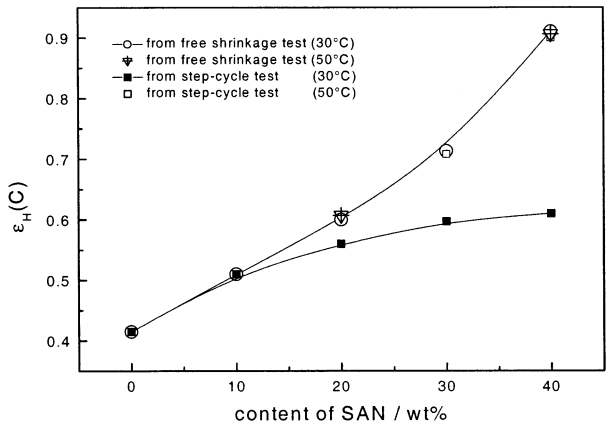

Figure 23. PCL/SAN blends: locations of the critical point C as derived from step-cycle and free shrinkage tests at 30 and 50 °C.

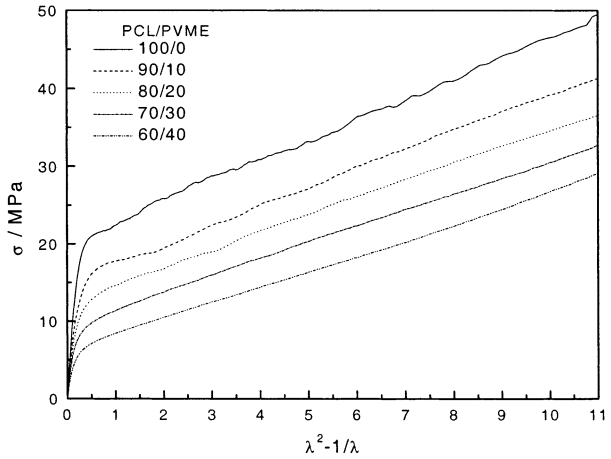

Figure 24. Curves of Figure 11 represented as σ vs the rubber measure of strain $\lambda^2 - 1/\lambda$ (Haward−Thackray plots).

decrease in the crystallinity, i.e., in the fraction occupied by the skeleton of crystal blocks, does not change the critical strains ϵ_H(A) and ϵ_H(B). A variation of the crystallinity shows only up in the critical stresses. Here we find the same behavior which confirms the generality of this property.

Different from A and B, point C which marks the begin of a disintegration of the crystal blocks represents a property of both the crystals via their binding energy and the entanglement network via the stress produced in it. Hence, if the network topology, i.e., the entanglement density in the amorphous regions is varied, we also expect a shift in the location of the critical point C. In this respect the two mixtures obviously differ from each other. As it appears, the swelling of the amorphous regions with the flexible PVME chains does not change the entanglement density, whereas an inclusion of the stiffer SAN chains results in its reduction. This reduction shows up directly when we represent the true stress−strain curve $\sigma(\epsilon_H)$ in the form suggested by Haward and Thackray,[22,23] namely as σ vs the strain measure of rubbers

$$\lambda^2 - 1/\lambda$$

as is shown in Figure 24 for PVME and Figure 25 for SAN. These Haward−Thackray plots express the view that cold drawing of semicrystalline polymers resembles above the yield point a drawing of a network—the

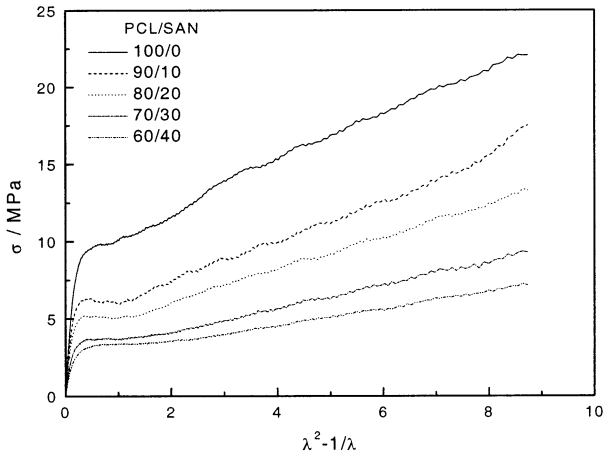

Figure 25. Curves of Figure 14 represented as Haward−Thackray plots σ vs $\lambda^2 - 1/\lambda$.

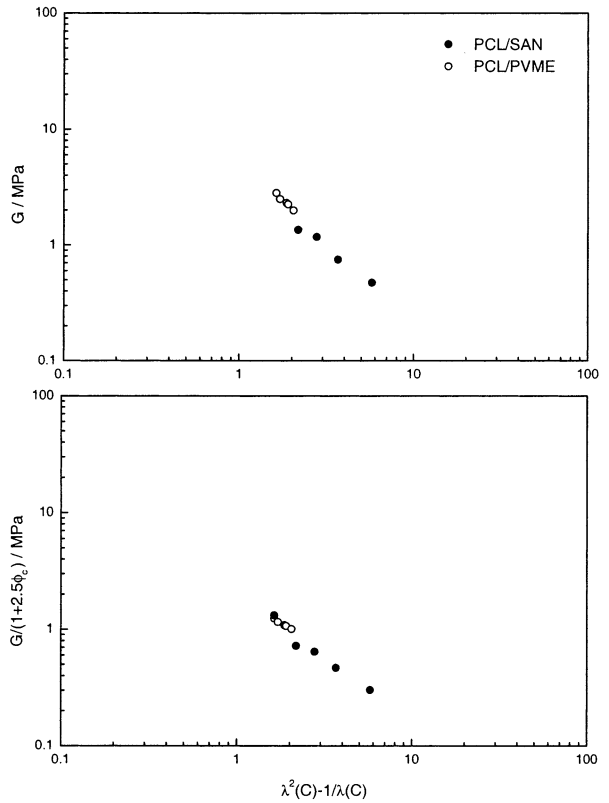

Figure 26. PCL/SAN and PCL/PVME blends: shear modulus of the entanglement network G deduced from the final slopes in Figures 25 and 24 plotted vs the rubber measure of strain at C (top). In the bottom figure G is modified to account for the filler effect of the crystallites.

entanglement network—under conditions of a high inner viscosity. The plots in fact produce a linear relation between σ and $\lambda^2 - 1/\lambda$ above the yield point, thus confirming this view. The slopes in the plots relate to the shear modulus G of the entanglement network. As one notes, for the PCL/PVME mixtures G shows only a minor reduction compared to the initital shear modulus associated with the PCL network, whereas the decrease in the PCL/SAN mixtures is much larger. In view of this behavior, one immediately understands why, in the mixtures with PVME, the critical strain ϵ_H-(C) is essentially invariant but shifts to higher values in the mixtures with SAN. At point C the network produces that stress which is necessary to begin with

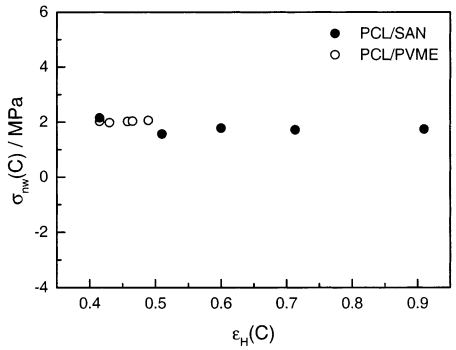

Figure 27. PCL/SAN and PCL/PVME blends: stress built up by the entanglement network at point C. Values follow from the corrected shear moduli in Figure 26 and the critical strains.

the disintegration of the crystal blocks. This will set in for those blocks which are oriented with their chains under 45° against the stretching direction, because these crystals experience the maximum resolved shear stress. For the PCL/PVME mixtures this critical stress is always reached at a strain $\epsilon_H = 0.41$ of the entanglement network. In the PCL/SAN mixtures which have a lower shear modulus G, a higher strain is necessary to reach this crystal stability limit.

One can check this condition in more detail. Figure 26 gives in the upper part the shear moduli deduced from the Haward−Thackray plots, plotted vs the rubber measure of strain at the respective points C for all the samples. If one wishes to compare these systems with normal rubbers, one has to account for the filling of the amorphous matrix with the crystallites and can try to do this in the same way as the presence of a filler material is accounted for in rubbers. The measured external stress as reflected in the value of G is higher than that produced by the amorphous network parts alone. To account for that, one can try to use the Einstein equation for a filled rubber

$$G = G_0(1 + 2.5\phi_c) \quad (1)$$

where G_0 denotes the modulus of the entanglement network and ϕ_c is the crystallinity as above. The values of G_0 thus estimated are given in the lower part of the figure. In a next step, using G_0 and the elongation ratio λ at the critical points C, one can estimate for all samples the network stresses σ_{nw} acting at C onto the crystallites. These values

$$\sigma_{nw}(C) = G_0(\lambda^2(C) - 1/\lambda(C))$$

are given in Figure 27. We obtain an essentially constant value of about 1.8 ± 0.2 MPa, which represents in our understanding the critical stress necessary to initiate the disintegration of the crystal blocks.

Acknowledgment. Funding of this work came from the Deutsche Forschungsgemeinschaft (Sonderforschungsbereich 428) and is gratefully acknowledged. Thanks are also due to the Fonds der Chemischen Industrie for financial help.

References and Notes

(1) Oudhuis, A. A. C. M.; Thiewes, H. J.; van Hutten, P. F.; ten Brinke, G. *Polymer* **1994**, *35*, 3936.
(2) Bisso, G.; Casarino, P.; Pedemonte, E. *Thermochim. Acta* **1998**, *321*, 81.
(3) Bisso, G.; Casarino, P.; Pedemonte, E. *Macromol. Chem. Phys.* **1999**, *200*, 376.
(4) Chiu, S. C.; Smith, T. G. *J. Appl. Polym. Sci.* **1984**, *29*, 1797.
(5) Keroack, D.; Zhao, Y.; Prud'homme, R. E. *Polymer* **1998**, *40*, 243.
(6) Koleske, J. V.; Lundberg, R. D. *J. Polym. Sci., Part A-2* **1969**, *7*, 795.
(7) Russell, T. P.; Stein, R. S. *J. Polym. Sci., Polym. Phys. Ed.* **1983**, *21*, 999.
(8) Mandal, T. K.; Woo, E. M. *Polym. J.* **1999**, *31*, 226.
(9) Woo, E. M.; Mandal, T. K. *Macromol. Rapid Commun.* **1999**, *20*, 46.
(10) Wang, Z.; Wang, X.; Yu, D.; Jiang, B. *Polymer* **1997**, *38*, 5897.
(11) Wang, Z.; Jiang, B. *Macromolecules* **1997**, *30*, 6223.
(12) Hiss, R.; Hobeika, S.; Lynn, C.; Strobl, G. *Macromolecules* **1999**, *32*, 4390.
(13) Hobeika, S.; Men, Y.; Strobl, G. *Macromolecules* **2000**, *33*, 1827.
(14) Men, Y.; Strobl, G. *J. Macromol. Sci., Phys.* **2001**, *B40*, 775.
(15) Al-Hussein, M.; Strobl, G. *Macromolecules* **2002**, *35*, 8515.
(16) Strobl, G.; Men, Y. *Abstr. Pap. Am. Chem. Soc.* **2002**, *223*, 233.
(17) Men, Y.; Strobl, G. *Chin. J. Polym. Sci.* **2002**, *20*, 161.
(18) Hauser, G.; Schmidtke, J.; Strobl, G. *Macromolecules* **1998**, *31*, 6250.
(19) Al-Hussein, M.; Strobl, G. *Macromolecules* **2002**, *35*, 1672.
(20) G'Sell, C.; Hiver, J.; Dahoun, A.; Souahi, A. *J. Mater. Sci.* **1992**, *27*, 5031.
(21) Heck, B.; Hugel, T.; Iijima, M.; Sadiku, E.; Strobl, G. *New J. Phys.* **1999**, *1*, 17.
(22) Haward, R.; Thackray, G. *Proc. R. Soc. London, A* **1968**, *302*, 453.
(23) Haward, R. *Macromolecules* **1993**, *26*, 5860.

MA025955B